Published: 26 November 2026 Volume 13 | Issue 2 | 809-822

OPEN ACCESS

Journal of Daylighting

Journal homepage: www.solarlits.com/journals/jd

RESEARCH ARTICLE

Daylight and Thermal Trade-offs of Glazing–Overhang Retrofits in a Hot-Coastal Educational Drawing Hall

Sameh A. Qadry *

Department of Architectural Engineering, Faculty of Engineering, Horus University, Egypt

Abstract

This study evaluates nine combinations of glazing and fixed horizontal overhangs (C1–C9) for a south-facing educational drawing hall in New Damietta, Egypt. On-site measurements of indoor air temperature were compared with simulations over six independent occupied monitoring days. The mean absolute error was 2.31°C and the root mean square error was 2.61°C, with a systematic warm bias that limits interpretation of absolute thermal conditions. Annual daylight performance was assessed by spatial daylight autonomy (sDA), annual sunlight exposure (ASE), and useful daylight illuminance (UDI). ASE was converted from DesignBuilder's passing-area output to conventional exposed area. A 1.00 m wide horizontal overhang, measured as its outward projection from the façade, reduced ASE exposure by 46.63–47.97% within each glazing family, although every case remained above the 10% reference limit. The decision method scores cooling demand alone in the energy domain, avoiding double counting of solar gains and cooling response. C9, comprising low-emissivity, argon-filled double glazing with a 1.00 m wide overhang, scored 97.42/100 and ranked first in all 45 tested category-weight combinations; its narrowest lead was 2.07 points. This identifies a stable comparative candidate within the tested matrix, rather than a universal optimum. Daylight predictions lack field validation, view-dependent glare remains unresolved, and the thermal evaluation does not establish equipment-level accuracy.

Keywords: Annual sunlight exposure, Climate-Based daylight modelling, Educational drawing hall, Façade retrofit

1. Introduction

Daylight is central to drawing and studio teaching because prolonged visual work depends on adequate illuminance across the workplane. In northern Egyptian coastal educational buildings, the same south-facing glazing that supplies useful daylight can expose workstations to direct sun and increase cooling loads. Classroom studies therefore show that greater daylight sufficiency may coexist with excessive annual sun exposure [1],[2]. Research on Egyptian teaching and office spaces likewise demonstrates the importance of façade configuration and orientation for visual and thermal performance [3],[4]. These findings establish the regional need for retrofit decisions that consider daylight, direct-sun exposure, cooling demand, and warm discomfort together.

Broader façade studies have examined larger parametric design spaces. Abedini et al. optimized shading types and window-to-wall ratio using spatial daylight autonomy (sDA), annual sunlight exposure (ASE), energy-use intensity, and thermal-comfort percentage in an office [5], while Abdelhamid et al. evaluated patterned screens for daylight and visual comfort in an Egyptian architecture studio [3]. Advanced-glazing and fixed-shading comparisons report similar energy–daylight coupling [6],[7]. Related multi-objective studies have extended these comparisons across school envelopes in different climates, hot-humid fenestration systems, and fixed sun-shading devices [8–10].

*Corresponding author.

Sqadry@horus.edu.eg (S. A. Qadry)

Received 28 August 2026; Revised 24 October 2026; Accepted 3 November 2026; Published online 26 November 2026

Copyright: © 2026 by the Author(s). Licensee Solarlits Limited (Hong Kong). This is an open access article distributed under the terms and conditions of the Creative Commons Attribution (CC BY) license.

Citation: Sameh A. Qadry, Daylight and Thermal Trade-offs of Glazing–Overhang Retrofits in a Hot-Coastal Educational Drawing Hall, Journal of Daylighting, 13:2 (2026) 809-822. doi: 10.15627/jd.2026.43

Nomenclature

ASE	*Annual Sunlight Exposure*
C1–C9	*Controlled façade cases*
DGP	*Daylight Glare Probability*
MAE	*Mean Absolute Error*
PMV	*Predicted Mean Vote*
COP	*Coefficient of Performance*
SHGC	*Solar Heat Gain Coefficient*
PPD	*Predicted Percentage Dissatisfied*
RMSE	*Root Mean Square Error*
sDA	*Spatial Daylight Autonomy*
UDI	*Useful Daylight Illuminance*
WWR	*Window-to-wall ratio*
HVAC	*Heating, Ventilation and Air Conditioning*
VLT	*Visible Light Transmittance*

Egyptian educational buildings add an orientation-sensitive thermal context [4]. This literature establishes the trade-off and shows that parametric weighting by itself is not a novel contribution.

In an existing drawing hall, orientation, window number, and opening dimensions are often fixed, leaving glazing replacement and external projection as the most buildable façade interventions. The present study combines a bounded occupied-period temperature evaluation with a controlled 3 × 3 façade matrix, corrects the reporting direction of ASE, examines occupied-hour temperature tails rather than relying only on annual means, and tests the preference sensitivity of the resulting ranking. The contribution is a transparent decision procedure for a constrained retrofit; it is neither a formal calibration nor a universal optimization model.

The study examines a south-facing drawing hall on the uppermost occupied floor of Horus University. It asks how three glazing systems and three fixed-overhang depths alter daylight, direct-sun exposure, cooling demand, and modelled comfort; which heat-balance terms explain the cooling response; and whether the preferred alternative remains stable when daylight, cooling, and comfort priorities vary. Figure 1 summarizes the evidential and decision sequence.

2. Materials and methods

2.1. Case-study boundary and field documentation

Drawing Hall 1 is on the third and uppermost occupied floor of the Faculty of Engineering at Horus University, New Damietta, Egypt (approximately 31.55°N, 31.10°E). Its principal external façade faces south. The hall was selected because it combines sustained drawing tasks, four large south-facing windows, long occupied periods, and roof exposure. Conclusions are restricted to this documented room; no comparison is made with unmonitored rooms elsewhere in the building.

The surveyed room plan is 17.00 m × 8.00 m. DesignBuilder uses a 4.00 m block height; its reported thermal-zone volume (499.666 m^3) and net floor area (133.2443 m^2) give an internal model height of approximately 3.75 m. The DesignBuilder geometry reports 140.894 m^2 for the floor/roof surface, whereas the annual daylight grid covers 133.244 m^2 after the program's workplane and perimeter rules; these quantities are therefore reported separately. Four fixed openings are arranged on the south façade. Each is 3.00 m wide and 2.20 m high, with a sill 1.00 m above the floor and 4.00 m centre-to-centre spacing. Figure 2 combines the site and floor-plan context with the sensor position and acquisition assembly; Figure 3 records the existing façade and baseline envelope.

2.2. Thermal and daylight models

The model was prepared in DesignBuilder 7.0.2.6. Thermal calculations used EnergyPlus 9.4.0.002 and annual daylight calculations used Radiance. All cases used EGY_AL ISKANDARIYAH_ALEXANDRIA_ETMY.epw (Alexandria, World Meteorological Organization (WMO) station 623180; 31.20°N, 29.95°E; elevation 7 m; UTC+2, Coordinated Universal Time). The file header identifies an Egyptian typical meteorological year developed from 1980–2003 observations. It was the available northern Egyptian Mediterranean coastal file and was applied identically to the nine controlled façade cases (C1–C9); it was not treated as measured New Damietta weather or as the outdoor record for the July monitoring campaign.

Table 1 consolidates the occupancy, schedule, lighting, cooling, and infiltration inputs. Occupant sensible gains were active in the annual EnergyPlus balance. Lighting and cooling followed the same Horus schedule: daylight-linked lighting responded to workplane illuminance, while cooling used a common autosized Simple HVAC/ideal-loads representation with a 24°C occupied cooling setpoint. The 28°C value is a setback setting, not the upper boundary of an occupied thermostat deadband. Mechanical outdoor-air supply and natural ventilation were off, but infiltration remained active. This shared HVAC abstraction was selected to isolate façade-driven load differences because measured equipment cycling, airflow, and electrical-power data were unavailable. The three installed split units are documented for the field campaign and were not represented as individual equipment components in the comparative annual runs. The resulting cooling outputs support controlled load comparison, not equipment-level energy prediction.

https://dx.doi.org/10.15627/jd.2026.43

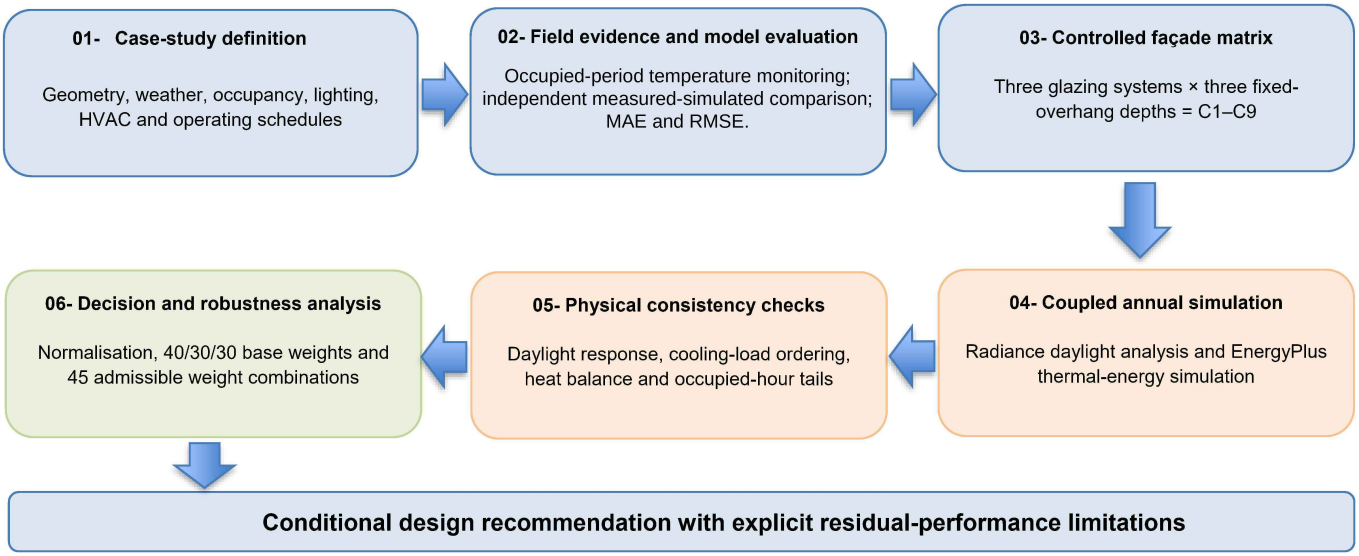

Figure 1. Evidence-led workflow from case-study documentation and independent model evaluation to controlled façade simulation, physical consistency checks and preference-sensitivity analysis.

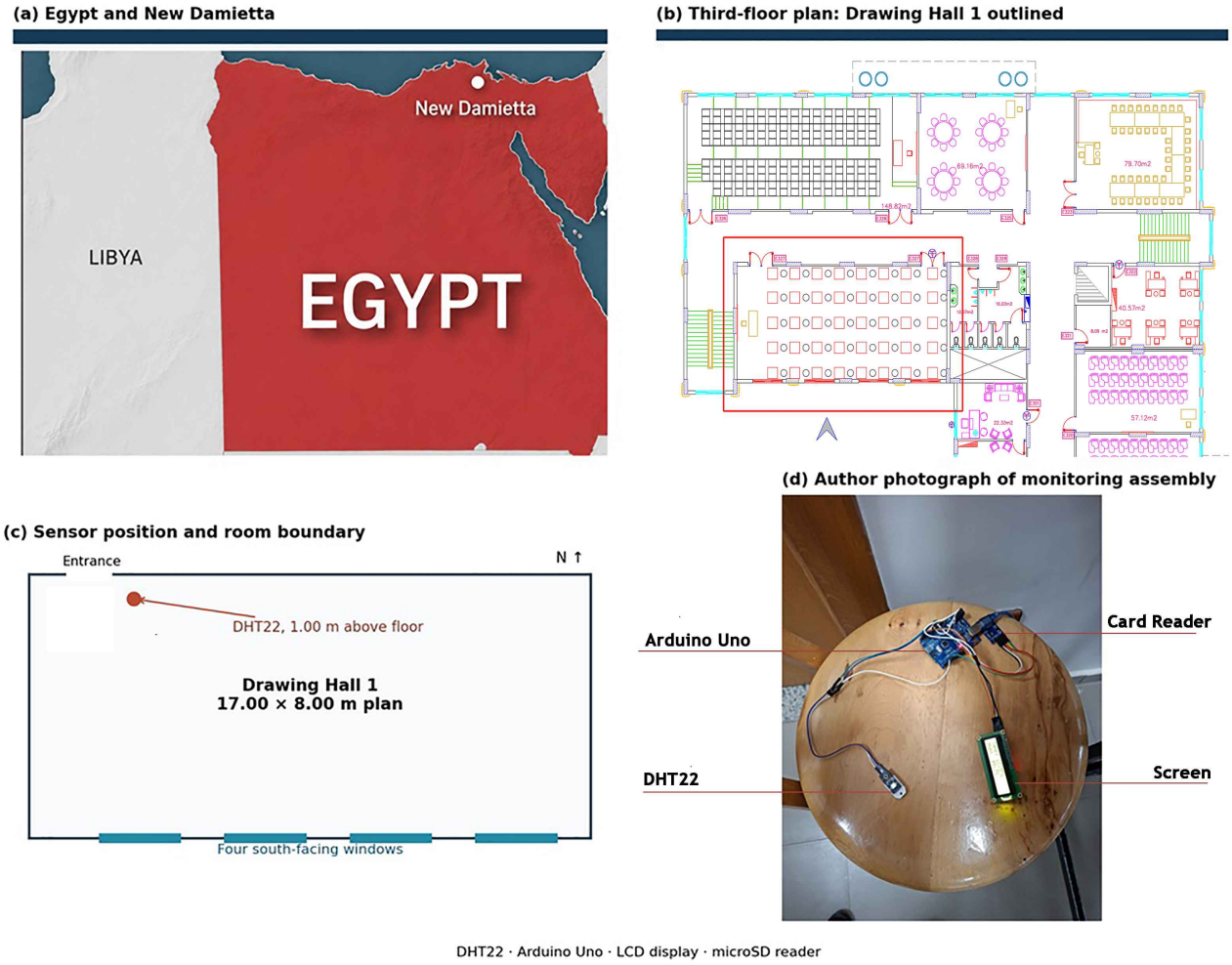

Figure 2. Case-study and monitoring documentation: (a) Egypt and New Damietta; (b) third-floor plan with Drawing Hall 1 outlined; (c) schematic sensor position beside the entrance, 1.00 m above finished floor and away from the south windows; and (d) author photograph of the DHT22–Arduino data-logging assembly.

https://dx.doi.org/10.15627/jd.2026.43

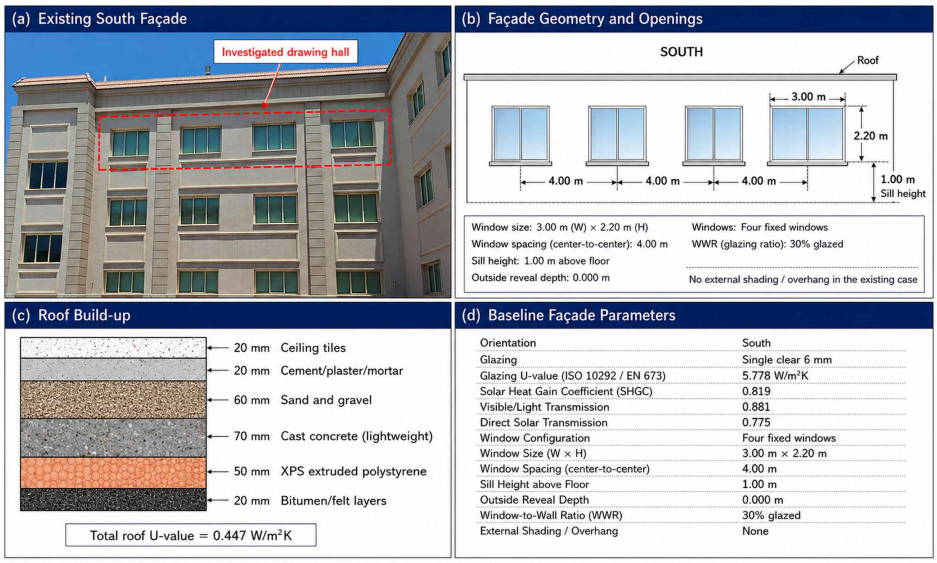

Figure 3. Existing south façade and baseline envelope data: (a) investigated hall, (b) opening geometry, (c) roof build-up, and (d) baseline façade parameters. Source: author survey and model inputs.

Table 1. Fixed model inputs and reporting boundary.

Parameter	Adopted setting
Simulation platform	DesignBuilder 7.0.2.6; EnergyPlus 9.4.0.002; integrated Radiance
Location and period	Building: New Damietta (31.55°N, 31.10°E); annual weather: EGY_AL ISKANDARIYAH_ALEXANDRIA_ETMY.epw, WMO 623180, 1980–2003 source period; 1 January–31 December
Room and façade	17.00 × 8.00 m surveyed plan; 4.00 m model block height; approximately 3.75 m internal zone height; 140.894 m² model floor/roof surface; 133.244 m² analysis grid; uppermost occupied floor; south-facing; WWR 30%
Windows	Four fixed openings; each 3.00 × 2.20 m; sill 1.00 m
Daylight grid	133.244 m²; 0.760 m workplane; 0.300 × 0.300 m grid; Good detail setting
Occupancy	0.248 person/m²; approximately 35 occupants; 140 W/person × 0.90 metabolic factor (approximately 1.20 met)
Schedule	09:30–16:00, Saturday–Thursday; Friday off; same Horus schedule applied to occupancy, lighting, and cooling availability
Lighting	16.50 W/m² at 500 lx (3.30 W/m² per 100 lx); linear daylight control; minimum input/output fractions 0.10/0.10
Cooling	Common autosized Simple HVAC/ideal loads; 24°C occupied cooling setpoint; 28°C setback, not an occupied deadband; COP 1.80; no mechanical outdoor air; infiltration active (0.712 ach occupied mean, 0.032 ach minimum)
Annual outputs	sDA, ASE, UDI; solar gains; sensible and total cooling; occupied-hour air and radiant temperatures; operative-temperature mean/95th percentile/maximum; relative humidity; PMV and PPD

2.3. Occupied-period temperature comparison

Indoor air temperature and relative humidity were recorded at one-minute intervals with one DHT22 sensor connected to an Arduino Uno, a liquid-crystal display (LCD), and a microSD logger (Figure 2d). The sensor was positioned 1.00 m above finished floor beside the entrance, away from direct solar exposure and supply-air discharge. Monitoring covered 09:30–16:00 on 15, 16, 18, 19, 20, 21, and 22 July 2026; the hall was closed on Friday 17 July. The original files contain 391 valid minute records per monitored day. Approximately 35 people were present, the three installed split systems operated with a 24°C thermostat setting, and the door and windows remained closed. These records describe conditions at one indoor point, rather than the spatial temperature distribution of the hall.

Blank trailing records were excluded without replacing valid observations. The existing comparison dataset groups the minute measurements into seven daytime observations per day: a first partial interval beginning at 09:30 and six subsequent hourly intervals beginning at 10:00–15:00. The single 16:00 endpoint does not form an additional hourly pair. The 18 July data were reserved for diagnosing the HVAC representation; the other six days supplied 42 measured–simulated pairs. No parameters were tuned against the independent set, so this exercise is termed an occupied-period model evaluation rather than calibration. A diagnostic run using aggregate nameplate capacity and rated efficiency was excluded from the C1–C9 ranking. No concurrent outdoor-weather, HVAC power, or airflow measurements were available, and the DHT22 had no laboratory calibration certificate.

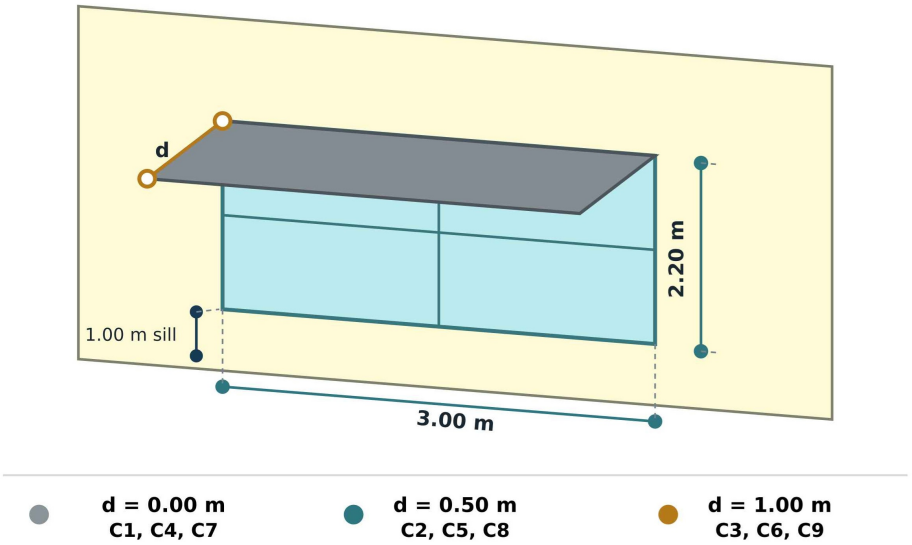

Figure 4. Fixed opening geometry and the three tested horizontal-overhang depths. The same depth was applied above each of the four south-facing windows.

Table 2. Controlled glazing and overhang matrix.

Case	Glazing construction	Overhang depth (m)
C1	Single clear, 6 mm (baseline)	0.00
C2	Single clear, 6 mm	0.50
C3	Single clear, 6 mm	1.00
C4	Clear air-filled double glazing, 6 mm/13 mm air	0.00
C5	Clear air-filled double glazing, 6 mm/13 mm air	0.50
C6	Clear air-filled double glazing, 6 mm/13 mm air	1.00
C7	Low-E argon-filled double glazing, 6 mm/13 mm argon (e2=0.1)	0.00
C8	Low-E argon-filled double glazing, 6 mm/13 mm argon (e2=0.1)	0.50
C9	Low-E argon-filled double glazing, 6 mm/13 mm argon (e2=0.1)	1.00

The resulting discrepancies therefore combine measurement, weather, timing, and model-representation uncertainty and cannot be assigned solely to the thermal solver.

With S(i) denoting simulated hourly air temperature, M(i) the corresponding measured value, and n the number of pairs, model–measurement differences were summarized using mean absolute error (MAE) and root mean square error (RMSE):

$$MAE = \frac{1}{n}\sum_{i=1}^{n}|S_i - M_i| \quad (1)$$

$$RMSE = \sqrt{\frac{1}{n}\sum_{i=1}^{n}(S_i - M_i)^2} \quad (2)$$

MAE describes the typical absolute hourly difference, whereas RMSE gives greater influence to larger residuals [11,12]. The sign of the mean residual was retained to identify systematic bias. These statistics define the evidential boundary for interpreting annual temperatures; they are not used as a binary claim that the model is calibrated.

2.4. Controlled façade matrix

The scenario matrix is the full factorial combination of three glazing constructions and three fixed overhang depths. C1 is the existing single-clear, unshaded baseline. The glazing properties used in the model were: single clear glazing, 6 mm, U = 5.778 W/(m²·K), solar heat gain coefficient (SHGC) = 0.819, and visible light transmittance (VLT) = 0.881; clear air-filled double glazing, U = 2.665 W/(m²·K), SHGC = 0.703, and VLT = 0.781; and low-emissivity argon-filled double glazing, U = 1.493 W/(m²·K), SHGC = 0.568, and VLT = 0.745. The overhangs were fixed, opaque external shading elements with outward projection depths of 0.00, 0.50, or 1.00 m, a 0.10 m geometric thickness, zero solar transmittance, and 0.50 solar reflectance. Here, overhang width denotes the projection perpendicular to the façade, not its span along the 3.00 m wide window. Window number, size, position, frames, weather, schedules, internal gains, lighting control, and HVAC representation remained unchanged. Figure 4 illustrates the opening geometry and tested overhang depths, while Table 2 summarizes the controlled glazing and overhang matrix.

2.5. Annual daylight metrics and ASE reporting direction

The annual daylight workplane was 0.760 m above the floor with a uniform 0.300 m grid. Spatial daylight autonomy (sDA300/50%) is the percentage of the analysis area receiving at least 300 lx for at least half of occupied hours. Annual sunlight exposure (ASE1000,250 h) is the percentage exposed to more than 1000 lx of direct sunlight for more than 250 occupied hours. Useful daylight illuminance (UDI100–3000/50%) is the percentage of area within the 100–3000 lx range adopted in the DesignBuilder settings for at least half of occupied hours [13]. Reference [14] provides the original UDI formulation; the upper threshold here follows the declared simulation setting. The overhangs are fixed architectural elements, and no result is attributed to dynamic shading [13–15].

A reporting distinction is essential for ASE. In DesignBuilder's annual grid report, "ASE Area in Range" is the area that passes the criterion—that is, it does not receive direct sunlight above 1000 lx for more than 250 occupied hours [13]. The study therefore converted that passing percentage to the conventional exposed-area metric:

$$ASE\ exposure\ (\%) = 100 - ASE\ area\ in\ range\ (\%) \quad (3)$$

The equivalent exposed area in square metres was calculated as 133.244 m² minus the reported in-range area. This conversion changes the label and preference direction, not the underlying Radiance results.

The field campaign measured temperature and relative humidity only. The DHT22 does not measure illuminance or luminance, and no simultaneous work plane illuminance or outdoor luminous-condition records were collected. The thermal measurements therefore cannot validate the Radiance daylight model. The daylight results are reported as comparative simulations under common geometry, optical inputs, weather, and calculation settings, not as experimentally validated illuminance predictions. This is a separate limitation from the air-temperature discrepancy.

2.6. Thermal outputs and decision synthesis

Annual energy outputs were window solar gains, zone sensible cooling, and total cooling demand, with cooling reported as a positive demand magnitude. Thermal outputs were occupied-hour operative temperature, relative humidity, predicted mean vote (PMV), and predicted percentage dissatisfied (PPD). Comfort calculations used an indoor air velocity of 0.137 m/s, the DesignBuilder generic clothing schedule (0.50 clo in summer and 1.00 clo in winter), and a 140 W/person standing/walking activity rate multiplied by 0.90, equivalent to 126 W/person or approximately 1.20 met for a 1.80 m² body area. Relative humidity was calculated by the model, not imposed as a constant. PMV and PPD remain model-based indices and do not replace an occupant survey [16,17].

Four indicators entered the decision synthesis. The daylight domain used sDA (maximize) and ASE exposed percentage (minimize); the energy domain used total cooling demand (minimize); and the comfort domain used the absolute value of annual occupied-hour mean PMV (minimize). UDI, window solar gains, zone sensible cooling, operative temperature, relative humidity, and PPD were retained as diagnostics. Excluding solar gains from the energy score avoids scoring both a causal driver and its cooling response. Retaining UDI diagnostically avoids adding a second correlated annual illuminance term to the daylight score. Equations (4) and (5) were applied separately to each scored indicator. For case i and indicator x, x_{min} and x_{max} are its minimum and maximum over C1–C9; $b_i(x)$ is used when higher values are preferred, and $c_i(x)$ when lower values are preferred. Both functions return values from 0 to 1, and none of the four indicator ranges was zero.

$$b_i(x) = \frac{x_i - x_{min}}{x_{max} - x_{min}} \quad (4)$$

$$c_i(x) = \frac{x_{max} - x_i}{x_{max} - x_{min}} \quad (5)$$

The category scores were calculated explicitly from these normalized quantities using Eqs. (6)–(8). In these equations, a_i is ASE exposed percentage, Q_i is annual total cooling demand, and $\overline{PMV}_i$ is the annual mean over the 2,191 occupied hourly records. The comfort input is $|\overline{PMV}_i|$, not the mean of the absolute hourly PMV values. The factor 50 in Eq. (6) gives equal weight to the two daylight indicators and converts their mean to a 0–100 scale; the factor 100 does the same for energy and comfort. These category scores enter the base-weight composite score in Eq. (9).

$$D_i = 50\,[b_i(sDA) + c_i(a)] \quad (6)$$

$$E_i = 100\,c_i(Q) \quad (7)$$

$$T_i = 100\,c_i(|\overline{PMV}|) \quad (8)$$

$$S_i = 0.40\,D_i + 0.30\,E_i + 0.30\,T_i \quad (9)$$

For example, C9's normalized sDA is 0.8710: subtracting the nine-case minimum of 2.818% from 59.450% and dividing by the range of 65.017 percentage points gives this value. C9 also has the lowest ASE exposed percentage, so its inverse-normalized ASE value is 1. Its daylight score is consequently 93.55. The lowest cooling demand and smallest absolute mean PMV give C9 energy and comfort scores of 100. Applying the 40/30/30 weights in Eq. (9) gives 97.42 after rounding. All scores and sensitivity calculations retain the full-precision inputs.

The 40/30/30 weights are explicit study preferences rather than occupant-derived or standard-prescribed values. Daylight, energy, and comfort weights were varied from 20% to 60% in 5-point increments while summing to 100%, producing 45 feasible combinations. This tests ranking stability within the declared preference space, not sensitivity to uncertain model inputs. Min–max normalization can magnify small absolute differences, especially for mean PMV; a score of 100 identifies the best tested

Table 3. Measured–simulated occupied-period air-temperature comparison.

Evaluation set	n	Measured mean (°C)	Simulated mean (°C)	MAE (°C)	RMSE (°C)
Diagnostic day, 18 July	7	27.27	31.78	4.51	4.57
Independent evaluation, 6 days	42	29.20	31.51	2.31	2.61

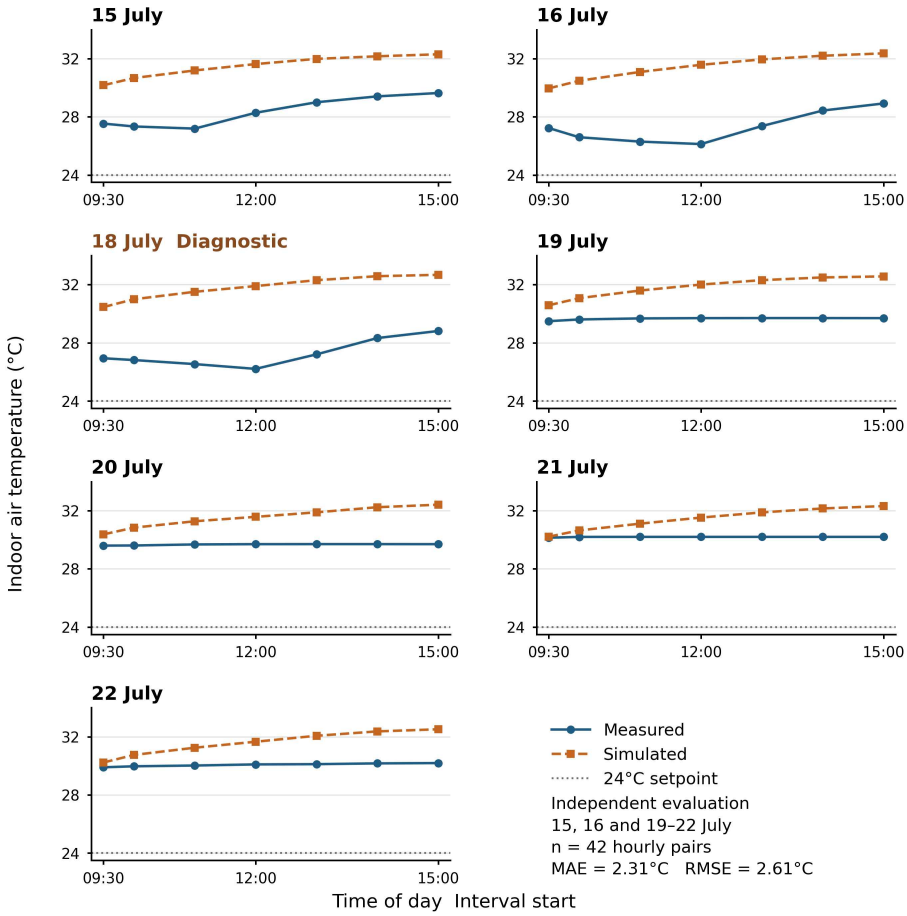

Figure 5. Separate hourly profiles of measured and simulated indoor air temperature for the seven monitored days in July 2026. Each panel uses the same time and temperature scales, and lines connect observations only within a day. The first observation represents the partial interval beginning at 09:30; the other observations represent intervals beginning at 10:00–15:00. The dashed line marks the 24°C cooling setpoint. The 18 July panel is diagnostic and excluded from the six-day independent statistics (42 pairs; MAE = 2.31°C; RMSE = 2.61°C). No observations are plotted for the closed Friday, 17 July.

alternative for that indicator, not 100% comfort or compliance [18,19].

3. Results and discussion

3.1. Baseline temperature comparison

Table 3 summarizes the measured-simulated temperature comparison, and Figure 5 presents separate hourly profiles for the seven monitored days. Across the six independent monitoring days, the baseline-temperature series used for the field comparison had a measured mean of 29.20°C and a simulated mean of 31.51°C. MAE was 2.31°C and RMSE was 2.61°C. All 42 residuals were positive. The diagnostic day showed a larger mean difference of +4.51°C. These values describe the evaluation series; they do not constitute validation of the annual autosized HVAC controller or its cooling-energy predictions.

Entering the aggregate nameplate capacity and rated efficiency in the Simple HVAC abstraction reversed the direction of the discrepancy. For the six independent days, mean simulated temperature became 24.14°C, with MAE 5.06°C and RMSE 5.22°C. The model remained near the thermostat setpoint and colder than measurements. Nominal capacity alone therefore did not reproduce field operation. Possible contributions include idealized control, delivered split-system performance, internal-gain timing, and the use of representative rather than concurrent outdoor weather. Absolute annual temperatures are consequently treated cautiously, whereas differences among cases retain value because all non-façade inputs are common.

Table 4. Annual daylight area metrics for the fixed 133.244 m² analysis grid, after conversion of ASE passing area to exposed area.

Case	sDA (%)	ASE exposed area (m²)	ASE exposed (%)	ASE area in range (%)	UDI (%)
C1	4.674	33.975	25.498	74.502	0.412
C2	12.990	27.473	20.619	79.381	3.918
C3	67.835	18.132	13.608	86.392	84.605
C4	3.230	33.792	25.361	74.639	0.137
C5	11.546	27.381	20.550	79.450	5.773
C6	60.687	17.766	13.333	86.667	86.460
C7	2.818	33.792	25.361	74.639	0.000
C8	11.271	27.381	20.550	79.450	5.292
C9	59.450	17.582	13.196	86.804	87.423

Note: These are annual qualifying areas or area percentages, not mean instantaneous illuminated areas. sDA and UDI identify the grid area meeting their illuminance criteria for at least 50% of occupied hours. ASE exposed area identifies the grid area exceeding 1000 lx of direct sun for more than 250 occupied hours. ASE exposed (%) = 100 - DesignBuilder ASE Area in Range (%). All percentages use the same 133.244 m² denominator.

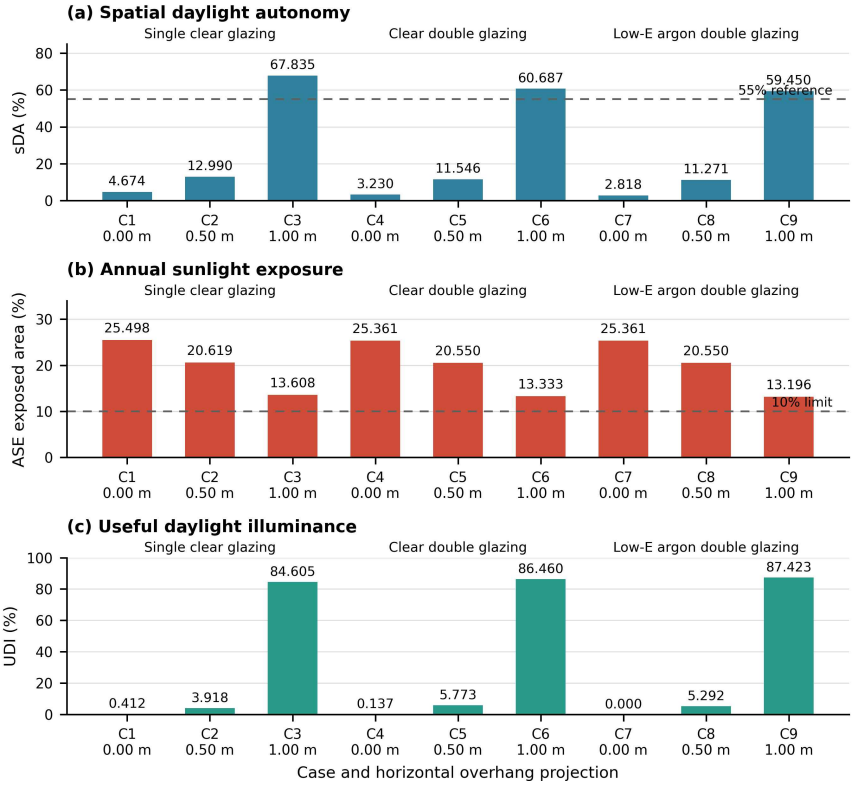

Figure 6. Annual daylight performance of C1–C9: (a) sDA, (b) conventional ASE exposed area, and (c) UDI. Dashed lines show the 55% sDA reference and 10% ASE exposure limit.

3.2. Daylight sufficiency and direct-sun exposure

Table 4 and Figure 6 summarize the annual daylight results for the nine facade cases. The 1.00 m overhang cases formed a distinct daylight group: each exceeded the 55% sDA reference and achieved UDI above 84%, whereas the unshaded cases remained below 5% sDA. This improvement coincided with a strong reduction in conventional ASE exposed area, indicating that the fixed projection redistributed annual illuminance while limiting prolonged direct-sun exposure. The result is specific to the stated Radiance settings and should not be interpreted as a dynamic-shading effect.

After converting DesignBuilder's passing-area output to exposed area, ASE decreased consistently with overhang depth. The 1.00 m projection reduced exposure by 46.63%, 47.43%, and 47.97% relative to the corresponding unshaded cases with single clear glazing, clear double glazing, and low-emissivity double glazing.

The improvement is substantial, but every case remains above the 10% reference; none is therefore ready for specification without supplementary direct-sun and view-based glare assessment. The daylight results should be read as a combined pattern rather than as sDA alone.

Table 5. Annual cooling and occupied-hour operative-temperature distribution summaries.

Case	Window solar gains (kWh)	Total cooling (kWh)	Mean operative temperature (°C)	95th percentile (°C)	Maximum (°C)
C1	15,095.22	16,934.60	25.58	27.07	27.65
C2	12,034.91	15,184.83	25.31	26.81	27.25
C3	9,880.85	14,016.81	25.10	26.55	27.16
C4	10,853.35	16,031.17	25.56	27.02	27.46
C5	8,738.93	14,612.19	25.31	26.76	27.29
C6	7,193.52	13,646.49	25.12	26.52	27.17
C7	8,333.78	15,198.92	25.45	26.87	27.36
C8	6,716.75	14,033.18	25.23	26.65	27.21
C9	5,532.82	13,241.39	25.07	26.45	27.15

Table 6. Signed occupied-period sensible heat-balance terms for the selected cases used to explain the cooling-load ordering.

Case	People (kWh)	Lighting (kWh)	Net windows (kWh)	Net infiltration (kWh)	Net opaque surfaces (kWh)	Zone sensible cooling (kWh)
C1	4697.5	479.0	11377.5	-5348.1	918.7	-12124.6
C3	4722.9	526.3	6514.2	-4973.3	2871.2	-9662.1
C7	4701.2	489.9	8856.3	-5237.4	1826.0	-10636.2
C9	4721.6	575.5	5512.0	-4959.1	3169.5	-9019.6

Note: Positive values add sensible heat to the zone; negative values remove it. Window, infiltration, and opaque-surface terms combine their reported heat-addition and heat-removal components. Small rounding differences occur because the source exports retain more digits.

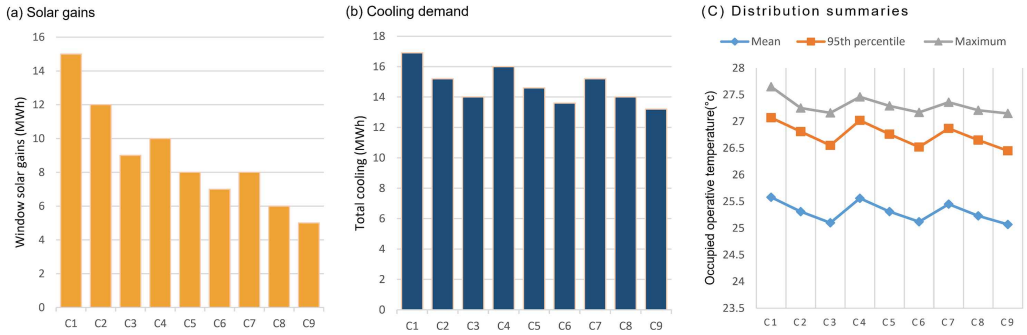

Figure 7. Energy and thermal response of C1–C9: (a) annual window solar gains; (b) annual total cooling demand, shown as a positive magnitude; and (c) mean, 95th-percentile, and maximum operative temperature over occupied hours. Energy is expressed in MWh and temperature in °C.

The deeper fixed projection increased sDA and UDI in the annual grid while reducing ASE exposure, but the calculation does not represent occupant view direction, luminance contrast, or workstation glare. Those unresolved visual conditions are treated as an implementation constraint rather than inferred from ASE.

3.3. Energy and thermal response

Table 5 and Figure 7 summarize the annual energy results and occupied-hour thermal response. Window solar gains decreased monotonically with overhang depth, by about one third between the unshaded and 1.00 m alternatives in each glazing family. The annual simulations produced physically ordered total cooling demand: deeper overhangs reduced cooling within every glazing family, and improved glazing reduced cooling at each common depth. C9 therefore recorded the lowest total cooling demand, while the unshaded single-clear baseline recorded the highest.

The detailed sensible heat balance explains the cooling-load ordering across the tested cases. For the specific C3–C7 comparison, the net window heat addition was 6.51 MWh in C3 and 8.86 MWh in C7; this difference outweighed C3's larger opaque-surface addition and the modest differences in lighting, people gains, and infiltration heat removal. The zone sensible cooling loads were consequently 9.66 MWh for C3 and 10.64 MWh for C7. Across C1, C3, C7, and C9, people gains remained near 4.7 MWh, confirming that metabolic heat was included, while infiltration provided net heat removal of about 5.0–5.35 MWh rather than being omitted. Table 6 reports the signed balance terms.

Annual means alone concealed the warm tail of the occupied-hour distribution. Across C1–C9, mean operative temperatures ranged from 25.07°C to 25.58°C, summer occupied means from 26.14°C to 26.51°C, 95th percentiles from 26.45°C to 27.07°C, and maxima from 27.15°C to 27.65°C. C9 was lowest for the mean, 95th percentile, and maximum; C6 had a very similar maximum.

Table 7. Occupied-hour PMV and PPD distribution summaries.

Case	Mean PMV	Mean PPD (%)	95th-percentile PMV	95th-percentile PPD (%)
C1	0.57	14.84	1.18	34.36
C2	0.51	13.54	1.13	31.79
C3	0.46	12.60	1.07	29.15
C4	0.57	14.70	1.17	33.83
C5	0.51	13.51	1.12	31.44
C6	0.47	12.64	1.07	29.35
C7	0.55	14.05	1.14	32.54
C8	0.50	13.08	1.10	30.56
C9	0.46	12.36	1.07	29.05

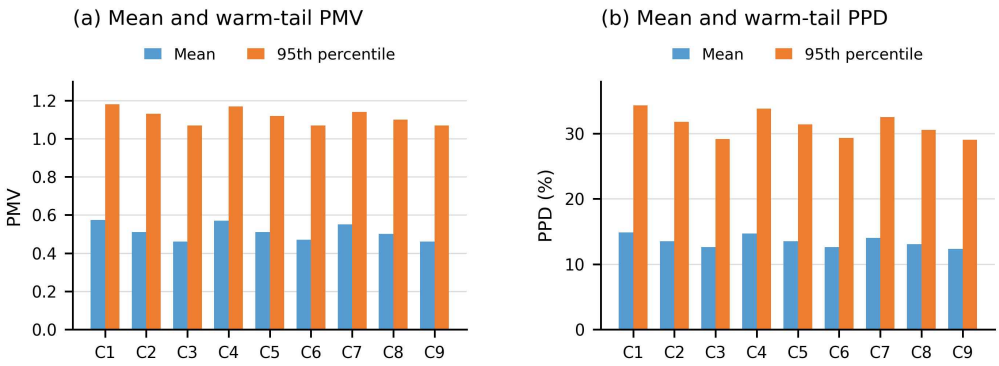

Figure 8. Occupied-hour thermal-comfort summaries for C1–C9 under common assumptions: (a) mean and 95th-percentile PMV and (b) mean and 95th-percentile PPD.

Table 8. Decision matrix; total cooling is the sole scored energy indicator.

Rank	Case	Daylight score	Energy score	Comfort score	Composite score
1	C9	93.55	100.00	100.00	97.42
2	C3	98.32	79.00	96.32	91.93
3	C6	93.94	89.03	91.44	91.72
4	C8	26.61	78.56	69.23	54.98
5	C5	26.82	62.88	55.22	46.16
6	C2	27.65	47.38	56.46	42.21
7	C7	0.56	47.00	25.95	22.11
8	C4	0.88	24.46	4.52	9.05
9	C1	1.43	0.00	0.00	0.57

Note: Category weights are 40% daylight, 30% total cooling demand, and 30% thermal comfort. Window solar gains remain diagnostic. Scores are relative to C1-C9 and were calculated from the full-precision simulation outputs; the source values presented in Tables 4, 5, and 7 are rounded for display.

Table 9. Representative results from the 45-combination category-weight sensitivity grid.

Weight scenario	D (%)	E (%)	T (%)	First	First score	Second	Lead
Base case	40	30	30	C9	97.42	C3	5.49
Daylight priority	50	25	25	C9	96.78	C3	3.78
Energy priority	25	50	25	C9	98.39	C6	7.53
Comfort priority	25	25	50	C9	98.39	C3	5.90
High daylight	60	20	20	C9	96.13	C3	2.07
High energy	20	60	20	C9	98.71	C6	8.22
High comfort	20	20	60	C9	98.71	C3	5.45

https://dx.doi.org/10.15627/jd.2026.43

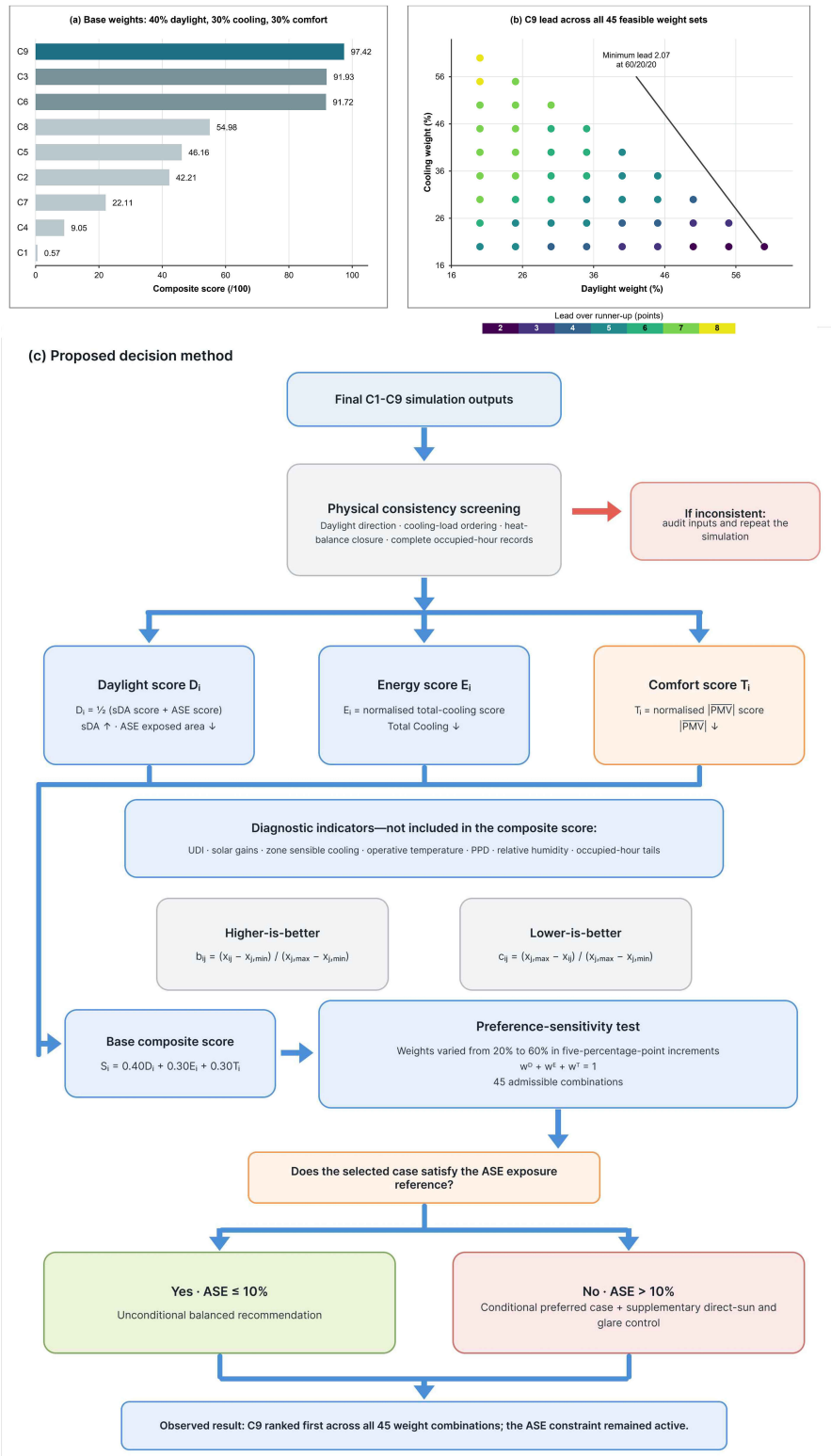

Figure 9. Decision analysis: (a) C1–C9 composite scores under 40/30/30 category weights; (b) C9's lead over the runner-up across all 45 feasible weight combinations; and (c) the proposed framework, which separates scored indicators from diagnostic evidence and prevents the composite rank from overriding the ASE limitation. Solar gains are diagnostic and are not included in the energy score.

These are controlled-model comparisons, not measured retrofit outcomes, and the field discrepancy does not provide a transferable numerical correction for their absolute temperatures.

The C1–C3 exports distinguish air-temperature control from the reported operative temperature. Across the same 2,191 occupied hourly records, mean air temperatures were 23.973, 23.946, and

23.911°C, whereas mean radiant temperatures were 27.194, 26.668, and 26.284°C. DesignBuilder reports operative temperature as the mean of air and radiant temperature [13], giving 25.584, 25.307, and 25.097°C, respectively. Most of the change in this mean therefore comes from the radiant component as the overhang projection increases, rather than from a different cooling setpoint. Small residual air-temperature differences are consistent with load-dependent hourly averages under scheduled, autosized cooling; these exports do not establish real compressor cycling or a physical thermostat hysteresis band. C2 and C3 are simulated alternatives, not separately monitored rooms.

3.4. Thermal-comfort indices

Table 7 and Figure 8 summarize the occupied-hour PMV and PPD distributions. Mean PMV and PPD followed the operative-temperature trend, with C9 giving the lowest annual occupied values. Their upper tails were materially warmer than the means: 95th-percentile PMV ranged from 1.07 to 1.18 and maximum PPD from 59.25% to 62.18%. The average indicators therefore should not be read as proof that all occupied hours were comfortable.

The common thermostat control reduces the scope for large differences in air temperature, so the comfort results should be interpreted as secondary, conditional evidence rather than independent proof of façade performance. PMV also depends on mean radiant temperature, humidity, air speed, clothing, and activity; controlling air temperature alone does not hold all these variables constant [13], [16], [17]. Mean occupied PMV changes only from about 0.575 in C1 to about 0.46 in C9. Its normalized score expresses that small relative difference, not a measured increase in occupant satisfaction. The single-point air-temperature evaluation does not validate radiant temperature, PMV, or PPD, and no occupant comfort survey was undertaken. The reported indices do not establish room-wide comfort at every workstation.

3.5. Decision matrix and sensitivity

Table 8 and Figure 9(a) present the composite scores and ranking under the 40/30/30 base weights. With solar gains and UDI retained as diagnostics rather than duplicate scored terms, C9 ranked first under the 40/30/30 base weights (97.42), followed by C3 (91.93) and C6 (91.72). C3 retained the highest sDA, whereas C9 had the lowest ASE exposed area, the highest UDI, the lowest cooling demand, and the mean PMV closest to zero. The ranking therefore reflects performance across the declared domains without separately scoring both solar gains and their cooling response.

C9 remained first in all 45 feasible category-weight combinations (Table 9; Figure 9(b)). Its narrowest lead was 2.07 points under the 60/20/20 daylight/energy/comfort weighting, where C3 was second. This consistency indicates robustness within the tested alternatives and weight bounds, but not beyond them. In particular, all cases still fail the ASE exposure reference. Figure 9(c) summarizes the decision framework.

3.6. Architectural interpretation and unresolved glare risk

Daltrozo et al. reported standardized classroom windows with sDA up to 98% but ASE up to 46%, whereas their irregular geometry limited exposure while often reducing daylight sufficiency [1]. Lim et al. identified 20–25% window-to-floor-ratio and glazing combinations with sDA near 96% and more than 40% lower solar exposure, but their cooling interpretation used an early-stage solar proxy rather than a dynamic thermal model [2]. In the present 30% WWR room, the 1.00 m overhang produced lower sDA (59.450–67.835%) but reduced ASE exposure to 13.196–13.608%, close to yet still above the 10% limit. These values are not a claim of outperforming the other studies; they locate the remaining direct-sun problem for a fixed existing façade.

Abedini et al.'s larger office optimization reached sDA up to 100% while evaluating multiple shading systems, WWR, and energy-use intensity [5], and Abdelhamid et al.'s patterned screens addressed daylight and visual comfort in an Egyptian architecture studio [3]. The present study compares only nine buildable retrofit cases, and its indoor-temperature comparison identifies limits on absolute thermal prediction. The daylight results remain simulation-based because no illuminance measurements were collected. Common inputs make the comparison traceable but do not remove uncertainty in the underlying models.

ASE is an annual area metric and should not be described as a direct measurement of glare. It does not represent occupant view direction, luminance distribution, contrast at drawing boards, or adaptation. The next architectural step is therefore a view-based daylight glare probability (DGP) analysis at representative seated and standing drawing positions, followed by tests of supplementary control such as exterior fins, perforated screens, or controllable blinds. Chi's classroom study shows that modest changes to roller-shade and louvre geometry can materially change daylight and visual performance [20]. Any added device must be tested against the sDA and UDI gains already obtained.

The physical and decision results support C9 as the strongest balanced candidate for the investigated room, while retaining C3 and C6 as comparators. C3 provides the highest sDA but has higher exposure and cooling demand, lower UDI, and a mean PMV slightly further from zero; C6 is the intermediate alternative with clear double glazing. C9's preference stability does not remove the need for an additional solar-control study, because the annual exposure threshold is not met and ASE cannot diagnose view-dependent glare.

Transfer beyond the investigated top-floor room requires caution. A comparable hall on the first or second floor would replace direct roof exposure with interzone heat exchange and would probably have lower absolute conductive cooling demand and a smaller warm-temperature tail. The façade solar and optical trends would still act in the same direction, but the relative C1–C9 cooling differences and the C9 decision margin cannot be assumed

unchanged because roof exchange, lighting response, and HVAC control interact nonlinearly. A floor-specific rerun is therefore required before extending the ranking. The six-day, single-sensor field evaluation, lack of concurrent outdoor and HVAC measurements, and use of a common ideal-loads system further bound absolute interpretation.

4. Conclusion

This study contributes a transparent method for combining daylight adequacy, excessive sun exposure, cooling demand, occupied-hour thermal tails, and comfort in a constrained educational-façade retrofit. Its main methodological contribution is the explicit conversion of DesignBuilder's ASE passing-area output to the conventional exposed-area metric and the separation of solar gains from the scored cooling indicator, supported by an explicit heat-balance check and weight-sensitivity analysis.

For the investigated south façade, a deep fixed overhang is necessary but not sufficient: it improves daylight distribution and reduces prolonged direct-sun exposure, yet the tested alternatives do not satisfy the ASE reference. Retrofit design should therefore pair the selected glazing–overhang geometry with a separately tested glare and direct-sun-control strategy rather than treating annual area metrics as proof of visual comfort.

Within the nine tested configurations, low-emissivity argon-filled double glazing with the deepest fixed overhang provides the most stable balance of the stated daylight, cooling, and warm-discomfort objectives. The comfort difference is small under the common thermostat control and remains model-based. This recommendation is conditional on the schedules, weather, ideal-loads HVAC representation, and top-floor boundary conditions; it should not be generalized to lower floors, other orientations, or different operating patterns without new simulation.

Future work should include workplane illuminance measurements with concurrent outdoor and sky-condition records to evaluate the daylight model, together with view-based glare analysis, seasonal thermal monitoring, HVAC power and airflow measurements, and an equipment-level system model. Lower floors require separate simulation because replacing roof exposure with interzone exchange can alter both absolute loads and relative façade effects. These steps would test the absolute predictions and the transferability of the comparative ranking.

Funding

This research received no external funding.

Contributions

S. A. Qadry: Conceptualization; Methodology; Investigation; Data curation; Formal analysis; Software; Validation; Visualization; Writing—original draft; Writing—review and editing; Project administration.

Data availability statement

The hourly comparison data, annual simulation outputs, decision calculations, and model documentation that support the findings are available from the corresponding author upon reasonable request.

Declaration of generative AI and AI-assisted technologies in the manuscript preparation process

OpenAI ChatGPT was used to assist with language editing, organization, and the graphical layout of selected author-supplied results. I independently verified all technical content, calculations, references, interpretations, and figure values. The tool was not used to generate or modify the measured data, simulation outputs, research design, or scientific conclusions. I made all scientific decisions and accept full responsibility for the submitted manuscript.

Declaration of competing interest

The author declares no competing interests.

References

[1] J. G. Daltrozo, N. L. Peiter, E. Gabriel, I. P. Santos, Evaluating daylighting gains from window geometry reconfiguration in a classroom under a subtropical climate, Journal of Daylighting, 13:1 (2026) 97-107.

[2] T. W. Lim, Y. Tongtuam, N. Ongsavangchai, Optimizing window-to-floor ratio and glazing for daylight and cooling in tropical educational buildings: A case study in Chiang Mai, Thailand, Journal of Daylighting, 13:1 (2026) 44-56.

[3] Y. M. S. Abdelhamid, S. M. Wahba, M. ElHusseiny, The effect of parametric patterned façade variations on daylight quality, visual comfort, and daylight performance in architecture studio-based tutoring, Journal of Daylighting, 10:2 (2023) 173-191.

[4] A. I. Elshamy, R. R. Moussa, M. Alghrieb, E. Elshazly, I. El Mahallawi, H. Safwat, Thermal performance variations of office spaces in educational buildings resulting from façade orientation: An Egyptian case study, Buildings, 15:19 (2025) 3437.

[5] M. H. Abedini, H. Gholami, H. Sangin, Multi-objective optimization of window and shading systems for enhanced office building performance: A case study in Qom, Iran, Journal of Daylighting, 12:1 (2025) 91-110.

[6] X. Hong, X. Yang, Y. You, F. Shi, F. Yang, C. Cui, Y. Gong, D. Qian, Comparative analysis of hydrogel-based thermotropic glazing and fixed horizontal overhangs in building performance, Building and Environment, 266 (2024) 112116.

[7] A. Mesloub, R. Hafnaoui, M. H. H. Abdelhafez, T. E. Seghier, L. Kolsi, N. Ben Ali, A. Ghosh, Multi-objective optimization of switchable suspended particle device vacuum glazing for comfort and energy efficiency in school typologies under hot climate, Case Studies in Thermal Engineering, 61 (2024) 105039.

[8] M. Talaei, H. Sangin, Multi-objective optimization of energy and daylight performance for school envelopes in desert, semi-arid, and Mediterranean climates of Iran, Building and Environment, 255 (2024) 111424.

[9] Z. Wu, Y. Xu, Z. Wang, Multi-objective optimization of energy, view, daylight and thermal comfort for building fenestration and shading systems in hot-humid climates, PLOS ONE, 20:6 (2025) e0325290.

[10] C. Pérez Carramiñana, Á. B. González Avilés, N. Castilla, A. Galiano Garrigós, Influence of sun-shading devices on energy efficiency,

thermal comfort and lighting comfort in a warm semi-arid dry Mediterranean climate, Buildings, 14:2 (2024) 556.
[11] T. O. Hodson, Root-mean-square error (RMSE) or mean absolute error (MAE): When to use them or not, Geoscientific Model Development, 15 (2022) 5481-5487.
[12] H. Johra, M. Schaffer, G. Chaudhary, H. S. Kazmi, J. Le Dréau, S. Petersen, Coherent description of 48 metrics to compare, validate and assess accuracy of building energy models and indoor environment simulations, DCE Technical Reports, No. 314, Department of the Built Environment, Aalborg University, Aalborg, Denmark, 2023, 37 pp.
[13] DesignBuilder Software Ltd., Daylighting metrics; Annual daylighting outputs and display options; Comfort analysis, DesignBuilder Help v7.0 and v7.3. https://designbuilder.co.uk/helpv7.3/Content/DaylightMetrics.htm; https://designbuilder.co.uk/helpv7.0/Content/AnnualDalylightingOutputsAndDisplayOptions.htm; https://designbuilder.co.uk/helpv7.0/Content/Comfort_Analysis.htm
[14] A. Nabil, J. Mardaljevic, Useful daylight illuminances: A replacement for daylight factors, Energy and Buildings, 38:7 (2006) 905-913. https://doi.org/10.1016/j.enbuild.2006.03.013.
[15] Illuminating Engineering Society, Approved method: IES spatial daylight autonomy (sDA) and annual sunlight exposure (ASE), ANSI/IES LM-83-23, New York, USA, 2023.
[16] ASHRAE, Thermal environmental conditions for human occupancy, ANSI/ASHRAE Standard 55-2023, ASHRAE, Peachtree Corners, GA, USA, 2023.
[17] International Organization for Standardization, Ergonomics of the thermal environment-Analytical determination and interpretation of thermal comfort using calculation of the PMV and PPD indices and local thermal comfort criteria, ISO 7730:2025, 4th ed., ISO, Geneva, Switzerland, 2025.
[18] D. M. Le, D. Y. Park, J. Baek, P. Karunyasopon, S. Chang, Multi-criteria decision making for adaptive façade optimal design in varied climates: Energy, daylight, occupants' comfort, and outdoor view analysis, Building and Environment, 223 (2022) 109479.
[19] J. Więckowski, W. Sałabun, Sensitivity analysis approaches in multi-criteria decision analysis: A systematic review, Applied Soft Computing, 148 (2023) 110915.
[20] D. A. Chi, Design adjustments for daylighting and visual comfort in a classroom with conventional shadings, Journal of Daylighting, 11:1 (2024) 165-180.

Disclaimer/Publisher's Note: The statements, opinions and data contained in all publications are solely those of the individual author(s) and contributor(s) and not of Solarlits and/or the editor(s). Solarlits and/or the editor(s) disclaim responsibility for any injury to people or property resulting from any ideas, methods, instructions or products referred to in the content.